Mode-Specific Vibrational Autodetachment Following Excitation of Electronic Resonances by Electrons and Photons

Cate S. Anstöter[1], Golda Mensa-Bonsu,[1] Pamir Nag,[2] Miloš Ranković,[2] Ragesh Kumar T. P.,[2]
Anton N. Boichenko,[3] Anastasia V. Bochenkova,[3,*] Juraj Fedor,[2,†] and Jan R. R. Verlet[1,‡]

[1]*Department of Chemistry, Durham University, Durham DH1 3LE, United Kingdom*
[2]*J. Heyrovský Institute of Physical Chemistry, Czech Academy of Sciences, Dolejškova 3, 18223 Prague 8, Czech Republic*
[3]*Department of Chemistry, Lomonosov Moscow State University, 119991 Moscow, Russia*

Electronic resonances commonly decay via internal conversion to vibrationally hot anions and subsequent statistical electron emission. We observed vibrational structure in such an emission from the nitrobenzene anion, in both the 2D electron energy loss and 2D photoelectron spectroscopy of the neutral and anion, respectively. The emission peaks could be correlated with calculated nonadiabatic coupling elements for vibrational modes to the electronic continuum from a nonvalence dipole-bound state. This autodetachment mechanism via a dipole-bound state is likely to be a common feature in both electron and photoelectron spectroscopies.

Processes involving the formation of electronic resonances are of fundamental importance in many fields of science and technology, ranging from astrophysics to biology and from electrical power distribution to semiconductor fabrication [1]. For many decades, transient electron capture and detachment have been studied by electron energy loss (EEL) spectroscopy [2], where the resonance is formed by an electron, with initial energy ε_i, colliding with a molecule M:

$$M + e^-(\varepsilon_i) \rightarrow M^{-*} \rightarrow M(\varepsilon_v) + e^-(\varepsilon_f).$$
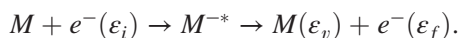
Upon M^{-*} resonance formation, two types of vibrational excitation are generally identified [2]. The first is the excitation of specific vibrational modes, where the electron loses the energy corresponding to a given vibrational quantum, leading to a final energy ε_f that is lower than ε_i by this specific energy loss ε_v. The second mechanism is an unspecific vibrational excitation, where energy is randomized over the nuclear degrees of freedom and the electrons are emitted statistically with a thermal distribution (thermionic emission) [3]. With the recent introduction of two-dimensional (2D) EEL [4–6], a third type of emission has been observed in several molecules, in which electrons are emitted with low (but finite) constant ε_f over a range of ε_i and the spectra show vibrational structure [4,7]. Such detachment is inconsistent with either of the two excitation types, and no explanation has been provided so far.

More recently, 2D anion photoelectron (PE) spectroscopy has been used to provide complementary information to 2D EEL spectroscopy [8,9]:

$$M^- + hv \rightarrow M^{-*} \rightarrow M(\varepsilon_v) + e^-(\varepsilon_f).$$
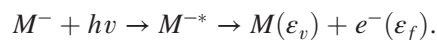
Although the initial geometry of the resonance M^{-*} is different than in electron attachment, the same two types of excitation or emission are usually considered. A structured PE signal with low and constant ε_f has also been seen over a range of hv in a number of targets, and this structure has been related to autodetachment from nonvalence states [10–12]. Here, we probe the electron detachment from electronic resonances in nitrobenzene (NB) using both 2D EEL and 2D PE spectroscopy in an attempt to gain insight into this structured low-energy electron emission channel. We show that signals are observed using both methods over a wide range of ε_i, despite the difference in geometric and electronic structure of the initial species. We suggest a mechanism for this emission which involves the nonvalence dipole-bound state (DBS) of the NB anion.

The 2D EEL spectroscopy was performed on an electrostatic spectrometer [13,14], where the incident electron beam is produced in a hemispherical electron monochromator and crosses the effusive beam of the neutral NB molecules at a temperature of 330 K. The scattered electrons are analyzed by a second hemispherical analyzer. The scattering angle has been fixed at 135°, and the electron energy resolution was 17 meV. The 2D EEL spectrum was constructed from individual EEL spectra taken at ε_i with 10 meV increments.

The 2D PE spectroscopy was carried out in an anion PE spectrometer that has been detailed previously [15]. Mass-selected NB$^-$ was produced in a molecular beam source and irradiated with light from a tunable nanosecond Nd: YAG pumped optical parametric oscillator providing ≈5 ns

pulses. Photodetached electrons were collected using a velocity-map imaging PE spectrometer with a spectral resolution <3% of ε_f. The 2D PE spectrum was constructed by taking PE spectra over $1.2 \leq hv \leq 3.0$ eV with 25 meV intervals.

We additionally performed electronic structure calculations using extended multiconfiguration quasidegenerate perturbation theory [16,17] with an active space including the π orbitals and also an active space including the relevant n orbitals (see Fig. S1 [18]). Vertical excitation energy (VEE) calculations from either the neutral or anion geometry were performed to estimate energies of valence excited states. The calculations used the (aug)-cc-pVTZ basis set, where the augmented functions were affixed only to the oxygen atoms. The vertical detachment energy was determined by adding a p-type function with a 10^{-10} exponent to the active space in order to mimic electron detachment. The position of a nonvalence dipole-bound state with respect to the detachment threshold, its equilibrium geometry, and nonadiabatic couplings with discretized continuum states were computed using an active space additionally augmented with a subset of diffuse orbitals of A_1 symmetry. Full details and computational results are provided in Supplemental Material [18].

The 2D EEL and 2D PE spectra for NB are shown in Figs. 1(a) and 1(b), respectively. To aid the comparison, we made two modifications to standard ways of plotting these spectra. First, the horizontal axis of the 2D EEL spectra is ε_f and not the electron energy loss ($\varepsilon_i - \varepsilon_f$), as usually presented [4,25]. Second, the vertical axis of 2D PE spectra is not hv but has been converted to $\varepsilon_i = hv - \text{AEA}$ [8]. $\text{AEA} = 0.95 \pm 0.03$ eV is the adiabatic electron affinity determined from the PE spectra, in good agreement with a previous PE spectrum [26]. Note also that the PE spectra have been normalized to total integrated signal levels to emphasize spectral changes as a function of the excitation energy.

The diagonal features in Fig. 1 have $\varepsilon_f = \varepsilon_i$ and $\varepsilon_f = \varepsilon_i - \varepsilon_v$, where ε_v is a constant energy left in the neutral. These correspond to specific vibrational excitation. In the 2D PE spectrum, diagonal features indicates direct detachment, whereby the intensity profile of specific ε_v levels in the neutral are determined by Franck-Condon factors between the anion and neutral ground state [27]. In the 2D EEL spectrum, the $\varepsilon_f = \varepsilon_i$ diagonal is the elastic scattering ridge, with parallel features corresponding to vibrational excitation of ε_v quanta in the neutral. In both spectroscopies, the formation of resonances can be identified by changes in the behavior of the diagonal signals. In the 2D PE spectrum, this can be seen clearly at $\varepsilon_i \geq 1.3$ eV. In 2D EEL, two resonances can be seen, centered around ~0.5 eV and ~1.5 eV (see Fig. S4 [18]), in agreement with positions seen in electron transmission spectroscopy (0.55 and 1.36 eV) [28,29] and in electron attachment spectroscopy (0.4 and 1.25 eV) [28,30].
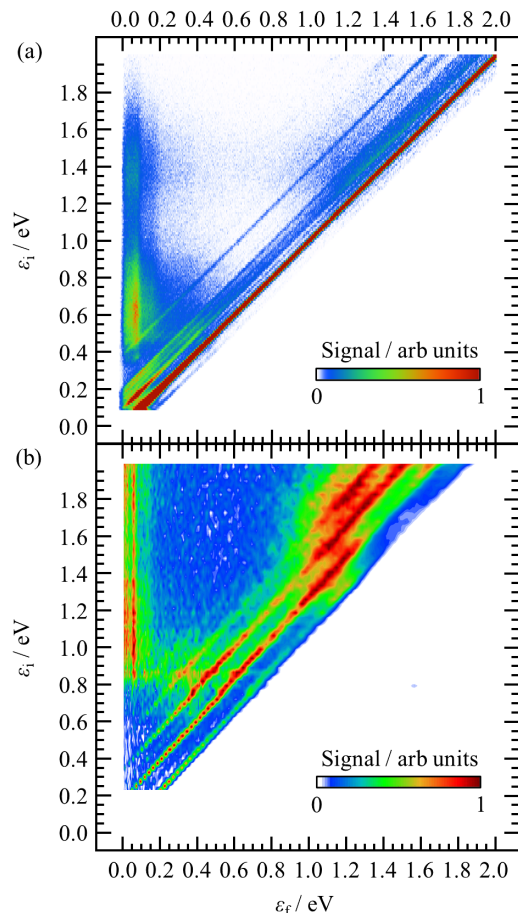

FIG. 1. (a) 2D electron energy loss spectrum of the nitrobenzene molecule and (b) 2D photoelectron spectrum of the nitrobenzene anion. The elastic ridge has been saturated for clarity and is shown in more detail in Fig. S4 [18].

In addition to the expected features, Fig. 1 also shows the electron signal with constant $\varepsilon_f < 0.2$ eV over a broad range of ε_i. Figure 2(a) shows the EEL spectrum, separately recorded at $\varepsilon_i = 0.8$ eV to attain high signal to noise, highlighting this spectral region. Figure 2(b) shows the average of PE spectra over the range $0.8 < \varepsilon_i < 2.0$ eV. Individual spectra at low energy are the same, and the average simply offers better signal to noise. Both spectra are broadly similar with a sharp peak at $\varepsilon_f = 60$ meV and a broad peak with a rough maximum at $\varepsilon_f \sim 130$ meV. The difference between the EEL and photoelectron spectrum at very low energies is most probably due to the different electron analyzers used; the hemispherical analyzer in the EEL experiment has a low transmission at very low ε_f.

Low ε_f emission is common in polyatomic molecules due to ultrafast conversion of resonances to the vibrationally hot anion ground state, which then emits electrons statistically. Because of the statistical nature, such emission should not display vibrational structure [31–33] and is inconsistent with the signal in Fig. 2. Nevertheless, the observation of this signal in both PE and EEL spectra
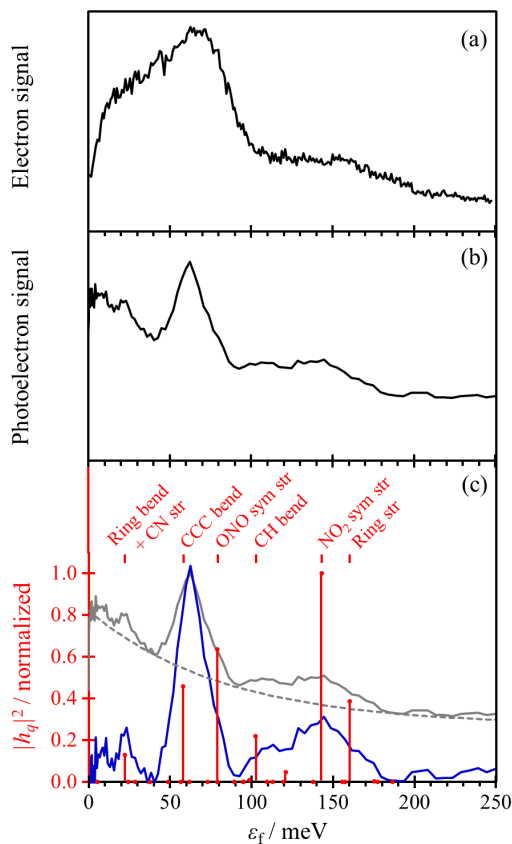
FIG. 2. (a) Low ε_f part of the EEL spectrum at $\varepsilon_i = 0.8$ eV. (b) Low ε_f part of the PE spectra averaged over the range $0.8 < \varepsilon_i < 2.0$ eV. (c) Comparison of data in (b) (gray solid line) to the norm-squares of the nonadiabatic coupling elements of h_q (red bars), with harmonic frequencies displaced by $E_{DBS} = -27$ meV. The blue line is the PE signal with smoothly varying background (gray dashed line) subtracted. Dominant vibrational modes are labeled (nomenclature sym = symmetric; str = stretch), and all modes are in the molecular plane.

across a range of ε_i suggests that it arises from a single emission channel. To address the origin of these well-defined low ε_f peaks, we first consider the electronic structure and resonances involved (for details, see Fig. S2 [18]).

Modelli and Venuti [28] identified the resonances at 0.55 and 1.36 eV using electron transmission spectroscopy (ETS) as the two π^* shape resonances $^2A_2$ and $^2B_1$, respectively (NB has C_{2v} symmetry in both anion and neutral ground states). These energies are in reasonable agreement with our VEE calculations from the neutral (0.28 and 1.50 eV, respectively). The signal at low and constant ε_f in the 2D EEL spectrum is seen for $\varepsilon_i > 0.4$ eV, which coincides with the onset of the $^2A_2$ resonance, indicating that this is likely to be the lowest energy entrance channel. In the 2D PE spectrum, the analogous signal appears only at $\varepsilon_i > 0.8$ eV. The $^2A_2$ resonance is optically dark with a very weak oscillator strength for the transition from the ground state and is therefore not seen in Fig. 1(b).

Our calculations instead show that the onset of the low and constant ε_f in the 2D PE spectrum can be correlated with excitation to the $^2B_2$ Feshbach resonance located at 0.75 eV, which has a very broad Franck-Condon window. The optical electronic transition to this state is symmetry forbidden, but B_1 and B_2 vibrational modes make it vibronically allowed. Feshbach resonances are typically not manifested in EEL excitation curves of specific vibrational modes (diagonals), but here the $^2B_2$ state may reveal itself indirectly and could serve as an entrance channel for the signal at low and constant ε_f across a wide range of ε_i between 0.4 and 1 eV in the 2D EEL spectrum. The higher-lying $^2B_1$ shape resonance is optically bright and seen in both experiments. It also leads to the low and constant ε_f signal. Surprisingly, we conclude that essentially any entrance channel, be it photon or electron excited, leads to a common exit channel that produces the structured signal at low ε_f.

We have already excluded purely statistical emission as the origin of the structure at low ε_f. In principle, it could also originate from the autodetachment from a low-lying resonance. Our calculations suggest that emission from the $^2A_2$ resonance may be consistent with the observed vibrational structure, as its potential energy surface along the CN bond length is similar to the neutral ground state with a total reorganization energy of ~ 0.2 eV. This resonance is calculated to be at ~ 0.3 eV vertically above the neutral ground state, and, hence, the adiabatic energy gap between them does not exceed 0.1 eV. Therefore, autodetachment from the $^2A_2$ could be consistent with the most prominent low-energy peak observed at 60 meV. However, the EEL and ETS experiments [28] suggest that the $^2A_2$ resonance is located higher in energy by ~ 0.2 eV.

An alternative source of the low-energy electrons is vibrational autodetachment from a nonvalence state. The best-known example of a nonvalence state is a dipole-bound state (DBS), in which the excess electron is loosely bound in a diffuse s-type orbital, located off the positive side of the permanent dipole moment of the neutral molecule, $\boldsymbol{\mu}$ [34]. Because of the weak interaction between the dipole-bound electron and the valence electrons of the neutral core, the potential energy surface associated with the DBS is very similar to that of the neutral molecule. For neutral NB, $|\boldsymbol{\mu}| = 4.2$ D, which is in excess of the $|\boldsymbol{\mu}| \approx 2.5$ D required to observe such states experimentally. Indeed, Rydberg electron transfer experiments by Desfrançois et al. verified that NB^- has a DBS with an estimated binding energy of 28 meV [26]. Hence, the DBS of NB^- may be a candidate for the source of the observed structure. But why should this lead to structured emission, and which modes facilitate the emission?

As the DBS is bound by $\boldsymbol{\mu}$ of the neutral core, intuition suggests that the vibrational modes that modulate $\boldsymbol{\mu}$ lead to electron emission. These are the infrared (IR) active modes. More specifically, it is the nonadiabatic coupling between

the DBS state and the electronic continuum that drives the autodetachment [35]. Because the DBS is totally symmetric, nonzero couplings arise for vibrational modes of A_1 symmetry, and the change in μ should be parallel to μ (the molecular axis of NB). Based on this analysis, only one IR-active mode, $v_8(A_1)$, which is the C-NO$_2$ symmetric stretch, modulates the DBS binding energy. We have calculated the nonadiabatic coupling matrix elements h_q between state-averaged complete active space self-consistent field wave functions that describe the DBS (ψ_{N+1}) and the discretized continuum state ($\psi_{N,\varepsilon}$) near the detachment threshold at the DBS equilibrium geometry [35]:

$$h_q = \langle \psi_{N,\varepsilon} | \nabla_q | \psi_{N+1} \rangle_r,$$

where ∇_q is the nuclear momentum operator along the q normal mode and r are the electronic coordinates. In a simplified picture where two nondisplaced harmonic potentials describe the DBS and the neutral ground state along all normal modes (see Fig. 3), and assuming that h_q is independent of nuclear coordinates, the vibrational prefactor is the same for all modes and nonzero only if the final state has one less vibrational quantum. This gives the propensity rule associated with vibrational autodetachment from the DBS, which is to lose one quantum of vibrational energy, $\Delta v = -1$ [35,36].

The norm-squares of h_q are shown in Fig. 2(c) together with the spectrum from Fig. 2(b). The experimental spectrum also appears to have an unstructured thermal spectral component, and we have crudely subtracted an exponentially decaying function to represent this thermionic component, leaving the vibrational autodetachment spectrum. In order to make a correlation between $|h_q|^2$ and the emission spectrum, the positions of all the calculated harmonic frequencies must be displaced by approximately -27 meV. Given the $\Delta v = -1$ propensity, electron emission energies correspond to $\varepsilon_f = hv_e - E_{DBS}$, where the hv_e is the vibrational frequency of a given mode and E_{DBS} is the binding energy of the DBS (see Fig. 3). Hence, the
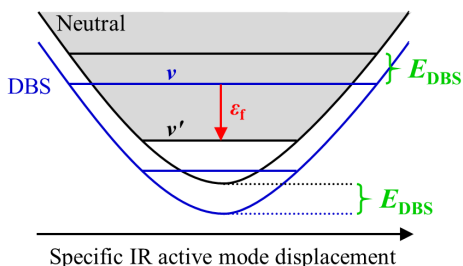
FIG. 3. Schematic of mode-facilitated electron loss from the DBS of the anion. Electron emission ε_f occurs from an IR-active vibrational mode of the DBS, v, by losing one quantum of vibrational energy to the neutral (black), $v' = v - 1$. The DBS (blue) and neutral (black) surfaces are offset by the DBS binding energy E_{DBS}.

displacement arises from the binding energy of the DBS, and we determine that $E_{DBS} \sim 27$ meV, in excellent agreement with the previous estimate by Desfrançois *et al.* of 28 meV [26]. Figure 2(c) confirms that the IR-active C-NO$_2$ symmetric stretch mode $v_8(A_1)$ leads to the largest nonadiabatic coupling between the DBS state and the electronic continuum.

There is a very good overall correlation between most peaks observed in the emission spectrum and the calculated $|h_q|^2$. However, the relative intensities do not agree as well. We note that a direct comparison might be misleading. First, the subtraction of the unstructured thermal spectral component, which contributes more toward lower frequency, may skew the overall intensities. Second, while the experimental peak at $\sim$130 meV is not the peak with the highest amplitude, its integrated signal (assuming the feature is a single peak) is, in fact, similar to that at 60 meV. Finally, the mode with the largest h_q may be manifested not only as the most prominent peak but also as the spectrally broadest peak, as the coupling to the continuum implies a more rapid decay. Taking all these observations together, we conclude that the most likely exit channel leading to the structured signal at low ε_f is vibrational autodetachment from the DBS of NB$^-$.

It is also tempting to simply compare an offset IR spectrum of NB to the vibrational autodetachment spectrum in Fig. 2. Such a comparison is shown in Fig. S3 [18]. As above, a good overall correlation between peak positions can be attained when a shift of -27 meV is applied to the IR spectrum. Although such a comparison has very different intensities, in line with the differing physical origins of the spectra, it provides a useful experimental tool and first indicator of the modes that are important and of the binding energy of the DBS.

There are two mechanisms by which the DBS can be populated. The first is by internal conversion through a conical intersection from a valence resonance [10–12]. For the second, a fraction of the population of the resonance internally converts to reform the vibrationally hot ground state of the anion, which could then populate the DBS. For example, the statistical sampling of all vibrational levels could lead to the transient formation of the DBS, which then undergoes rapid vibrational autodetachment. This second mechanism is supported by the smoothly decreasing background of the spectra in Fig. 2, which points to a thermionic contribution to the mode-specific autodetachment.

The electron emission mechanism described here can be compared with several processes involving the coupling of molecular vibrations with electrons in continuum. (i) In low-energy electron collisions with polar molecules, the IR-active modes are efficiently excited at the threshold via direct dipole excitation [37]. The autodetachment process described here can be, in principle, viewed as a reverse mechanism: The electron leaving the hot molecule via a nonvalence state deexcites specific modes.

(ii) Mode-specific vibrational autodetachment has been observed from nonvalence states populated by internal conversion from resonances; however, this emission occurs on a picosecond timescale and applies to resonances excited near the threshold [10–12]. (iii) Signatures of IR modes have also been seen in the direct photodetachment from nonvalence states. For example, Bailey *et al.* observed weak features in the PE spectrum of the dipole-bound anion CH_3CN^- that were redshifted by the IR modes of CH_3CN [38]. Similar features have been observed in the nonvalence correlation-bound state of $C_6F_6^-$, where both IR and Raman modes can contribute [39]. However, while this process similarly is based on nonadiabatic coupling between the nonvalence orbital and specific vibrations, the mechanism presented here fundamentally differs, as it is an autodetachment rather than photodetachment process. (iv) Lunt *et al.* observed a minimum in the total scattering cross section of electrons from NB around 0.1 eV [40], which they tentatively assigned to interference between a dipole-bound resonance and the direct scattering channel. While our results are not sensitive to such interference (the signal at $\varepsilon_f < 0.2$ eV cannot interfere with the direct channel), it does demonstrate that vibrational levels of the DBS serve as emission channels.

In conclusion, we have presented an interpretation of the origin of structure in low-energy electron loss channels observed in both electron energy loss and photoelectron spectroscopy. The structure observed in nitrobenzene arises from vibrational mode-specific electron loss from a nonvalence state of the anion and can be correlated with the IR-active modes of the neutral with A_1 symmetry, offset by the binding of a DBS. Our results provide a framework from which structured low-energy electron emission can be interpreted and highlight the ubiquity of nonvalence states in the dynamics of anions.

*bochenkova@phys.chem.msu.ru
†juraj.fedor@jh-inst.cas.cz
‡j.r.r.verlet@durham.ac.uk

[1] I. I. Fabrikant, S. Eden, N. J. Mason, and J. Fedor, in *Advances In Atomic, Molecular, and Optical Physics*, edited by E. Arimondo, C. C. Lin, and S. F. Yelin (Academic, New York, 2017), pp. 545–657.

[2] M. Allan, J. Electron Spectrosc. Relat. Phenom. **48**, 219 (1989).

[3] J. N. Bull, C. W. West, and J. R. R. Verlet, Chem. Sci. **6**, 1578 (2015).

[4] K. Regeta and M. Allan, Phys. Rev. Lett. **110**, 203201 (2013).

[5] F. Currell and J. Comer, Phys. Rev. Lett. **74**, 1319 (1995).

[6] T. Reddish, F. Currell, and J. Comer, J. Phys. E **21**, 203 (1988).

[7] M. Allan, M. Lacko, P. Papp, Š. Matejčík, M. Zlatar, I. I. Fabrikant, J. Kočišek, and J. Fedor, Phys. Chem. Chem. Phys. **20**, 11692 (2018).

[8] C. W. West, J. N. Bull, E. Antonkov, and J. R. R. Verlet, J. Phys. Chem. A **118**, 11346 (2014).

[9] C. S. Anstöter, J. N. Bull, and J. R. R. Verlet, Int. Rev. Phys. Chem. **35**, 509 (2016).

[10] J. N. Bull and J. R. R. Verlet, Sci. Adv. **3**, e1603106 (2017).

[11] J. N. Bull, C. W. West, and J. R. R. Verlet, Chem. Sci. **7**, 5352 (2016).

[12] J. N. Bull, C. S. Anstöter, and J. R. R. Verlet, Nat. Commun. **10**, 5820 (2019).

[13] M. Allan, J. Phys. B **25**, 1559 (1992).

[14] M. Allan, J. Phys. B **38**, 3655 (2005).

[15] J. P. Rogers, C. S. Anstöter, J. N. Bull, B. F. E. Curchod, and J. R. R. Verlet, J. Phys. Chem. A **123**, 1602 (2019).

[16] A. A. Granovsky, J. Chem. Phys. **134**, 214113 (2011).

[17] A. A. Granovsky, Firefly version 8.2.0, http://classic.chem.msu.su/gran/firefly/index.html.

[18] See Supplemental Material at http://link.aps.org/supplemental/10.1103/PhysRevLett.124.203401, which includes Refs. [19–24], for: computational details and results; a comparison of electron spectra with IR spectrum; and the full 2D EEL spectrum.

[19] M. J. Frisch *et al.*, *Gaussian 16, Revision A.03* (Gaussian, Inc., Wallingford, CT, 2016).

[20] J. Schiedt and R. Weinkauf, J. Chem. Phys. **110**, 304 (1999).

[21] A. A. Kunitsa and K. B. Bravaya, J. Phys. Chem. Lett. **6**, 1053 (2015).

[22] A. A. Kunitsa, A. A. Granovsky, and K. B. Bravaya, J. Chem. Phys. **146**, 184107 (2017).

[23] A. Giussani and G. A. Worth, J. Chem. Theory Comput. **13**, 2777 (2017).

[24] M. W. Schmidt, K. K. Baldridge, J. A. Boatz, S. T. Elbert, M. S. Gordon, J. H. Jensen *et al.*, J. Comput. Chem. **14**, 1347 (1993).

[25] M. Ranković, P. Nag, M. Zawadzki, L. Ballauf, J. Žabka, M. Polášek, J. Kočišek, and J. Fedor, Phys. Rev. A **98**, 052708 (2018).

[26] C. Desfrançois, V. Périquet, S. A. Lyapustina, T. P. Lippa, D. W. Robinson, K. H. Bowen, H. Nonaka, and R. N. Compton, J. Chem. Phys. **111**, 4569 (1999).

[27] R. R. Corderman and W. C. Lineberger, Annu. Rev. Phys. Chem. **30**, 347 (1979).

[28] A. Modelli and M. Venuti, Int. J. Mass Spectrom. **205**, 7 (2001).

[29] N. L. Asfandiarov, S. A. Pshenichnyuk, V. G. Lukin, I. A. Pshenichnyuk, A. Modelli, and Š. Matejčik, Int. J. Mass Spectrom. **264**, 22 (2007).

[30] A. Pelc, P. Scheier, and T. D. Märk, Vacuum **81**, 1180 (2007).

[31] E. E. B. Campbell and R. D. Levine, Annu. Rev. Phys. Chem. **51**, 65 (2000).

[32] J. U. Andersen, E. Bonderup, and K. Hansen, J. Phys. B **35**, R1 (2002).

[33] C. L. Adams, K. Hansen, and J. M. Weber, J. Phys. Chem. A **123**, 8562 (2019).

[34] K. D. Jordan and F. Wang, Annu. Rev. Phys. Chem. **54**, 367 (2003).

[35] J. Simons, J. Am. Chem. Soc. **103**, 3971 (1981).

[36] G.-Z. Zhu and L.-S. Wang, Chem. Sci. **10**, 9409 (2019).

[37] Y. Itikawa, Int. Rev. Phys. Chem. **16**, 155 (1997).

[38] C. G. Bailey, C. E. H. Dessent, M. A. Johnson, and K. H. Bowen, J. Chem. Phys. **104**, 6976 (1996).

[39] J. P. Rogers, C. S. Anstöter, and J. R. R. Verlet, Nat. Chem. **10**, 341 (2018).

[40] S. L. Lunt, D. Field, J.-P. Ziesel, N. C. Jones, and R. J. Gulleye, Int. J. Mass Spectrom. **205**, 197 (2001).